Initial spindle positioning at the oocyte center protects against incorrect kinetochore-microtubule attachment and aneuploidy in mice

Jessica N. Kincade and Ahmed Z. Balboula*

Animal Sciences Research Center, University of Missouri, Columbia, MO 65211, USA

Running title: Central spindle positioning protects against aneuploidy

Keywords: Aneuploidy, Nucleus Positioning, Spindle Positioning, Oocyte, Meiosis

*Corresponding author: Ahmed Z. Balboula, Animal Sciences Research Center, University of Missouri, Columbia, MO 65211, USA, abalboula@missouri.edu

ABSTRACT

Spindle formation and positioning are two critical events that must be regulated tightly to avoid erroneous chromosome segregation. Following nuclear envelope breakdown (NEBD), the spindle is predominantly assembled centrally before migrating towards the cortex to allow the first asymmetric division. The biological significance of primary central positioning of the spindle has not yet been studied. Because the spindle forms where NEBD occurs, nucleus position greatly influences the site of spindle assembly. We find that nucleus positioning is a dynamic process that depends on maternal age. Moreover, we show that preferential initial spindle positioning at the oocyte center is an insurance mechanism to avoid premature exposure to cortical Cdc42 signaling that hinders proper kinetochore-microtubule attachments, thereby protecting against the development of aneuploid gametes. These findings will help in understanding why female gametes are notoriously associated with high rates of aneuploidy, the leading genetic cause of miscarriage and infertility in women.

32 **INTRODUCTION**

33 Infertility is a globally prevalent issue affecting approximately 122 million women worldwide [1].
34 Errors in chromosome segregation during meiosis result in aneuploidy, the leading genetic cause
35 of infertility, spontaneous abortion, and congenital birth defects such as down syndrome[2,3].
36 Aneuploidy occurs in females of all ages, but women of advanced age experience elevated risk
37 of aneuploidy [4]. Given that chromosome segregation errors occur most frequently in female
38 gametes (as opposed to male gametes), particularly within the first meiotic division (Meiosis I,
39 MI)[5,6], it is crucial to understand the molecular mechanisms regulating female MI.
40

41 Oogenesis is a complex process that begins during fetal development in female mammalian
42 species, shortly after conception. During late pregnancy, oocytes enter MI and duplicate their
43 chromosomes [7]. Shortly after birth, all germ cells undergo a prolonged arrest that is maintained
44 until puberty. Hormonal cues prior to ovulation stimulate a subset of oocytes to resume meiosis
45 [7]. In fully-grown prophase I-arrested oocytes, the nucleus (germinal vesicle, GV) localizes
46 mainly at the center [8]. *In vitro*, peripherally localized nuclei migrate towards the center of the
47 oocyte, regulated by a meshwork of cytoplasmic actin. This meshwork of cytoplasmic actin
48 creates a gradient of velocity (higher near the cortex, lower near the center) induced by Myosin
49 Vb activity and relocates the nucleus centrally through gentle movement governed by active
50 diffusion, rather than exerting a force on the nucleus [9-11]. However, the biological significance of
51 central nucleus positioning is largely unknown.
52

53 Upon meiotic resumption, prophase I-arrested oocytes undergo nuclear envelope breakdown
54 (NEBD). Throughout the NEBD process, the microtubule organizing centers (MTOCs) undergo

55 a three-step fragmentation before clustering and sorting into two dominant spindle poles that are
56 integral in forming a bipolar spindle at the center of metaphase I (Met I) oocytes [12-15]. The
57 spindle dictates the plane of cell division [16], and, therefore, must migrate to the oocyte cortex to
58 ensure the highly asymmetric meiotic division [16,17]. Extruding a small polar body through a
59 highly asymmetrical division is critical as it allows the egg to retain a majority of the
60 cytoplasmic store of maternal RNAs and proteins synthesized during the growth phase which are
61 essential for fertilization and early embryonic development [18,19]. However, the necessity of
62 central spindle assembly prior to cortical spindle migration is unknown.
63
64 Here we show that nucleus positioning is a dynamic process that is affected by maternal age. A
65 majority of oocytes collected from sexually mature mice had a centrally positioned nucleus,
66 whereas a majority of oocytes from prepubertal mice had a peripherally positioned nucleus. We
67 find that peripheral nucleus positioning is associated with chromosome misalignment, abnormal
68 kinetochore-microtubule (K-MT) attachments and aneuploidy. Importantly, we find that central
69 spindle positioning post-NEBD is critical to avoid deleterious cortical Cdc42 signals that hinder
70 the fidelity of forming kinetochore-microtubule (K-MT) attachments, thereby protecting against
71 aneuploidy in mammalian eggs.
72

73 # RESULTS

74 ***Nucleus Positioning – A dynamic process***

75 Because the spindle forms where NEBD occurs whether at the center (Supplementary Fig. 1A)
76 or at the cortex (Supplementary Fig. 1B), we sorted full-grown prophase I-arrested oocytes
77 according to the positioning of the nucleus into three groups: central, intermediate, and

78 peripheral; herein after, these groups are referred to as central GV oocytes, intermediate GV
79 oocytes, or peripheral GV oocytes. Peripheral GV oocytes had a distance of 5 µm or less from
80 the nucleus to the nearest cortex, intermediate GV oocytes remained at a distance of 5 to 15 µm
81 from the nucleus to the nearest cortex, and central GV oocytes maintained more than 15 µm
82 distance from the nucleus to the nearest cortex (Fig. 1A). First, we observed the proportions of
83 these groups of oocytes *in vitro* after collection. Oocytes with a centrally located nucleus were
84 the most prevalent, contributing nearly 50.96% of all oocytes collected. Oocytes with an
85 intermediately positioned nucleus accounted for nearly 24.22% of all collected oocytes, while
86 peripheral oocytes represented only 24.81% of collected oocytes (Fig. 1B).
87 To determine whether nucleus positioning proportions *in vitro* are similar to those *in vivo*,
88 ovaries were collected at four ages (2 weeks, 3 weeks, 5 weeks, and 8 weeks) in order to display
89 nucleus positioning throughout reproductive development. All oocytes and their corresponding
90 nucleus positioning were examined from histological sections of ovaries stained with
91 Hematoxylin and Eosin (Fig. 1C,D). Similar to our *in vitro* results, ovaries from mice aged 8
92 weeks showed a majority of oocytes with a centrally positioned nucleus (63.52%). Interestingly,
93 younger mice (2 & 3 weeks of age) showed a majority of peripherally located nucleus (50.46%
94 and 55.63%, respectively), while mice aged 5 weeks showed very similar proportions of oocytes
95 with both a centrally and peripherally located nucleus (42.86% and 43.25%, respectively, Fig.
96 1D,E), suggesting that, before sexual maturation, oocytes have an eccentrically positioned
97 nucleus (likely incompetent) prior to central relocation after sexual maturation.
98
99 ***Oocytes with a peripherally located nucleus associate with higher rates of chromosome***
100 ***misalignment and aneuploidy***

101 Upon meiotic resumption, NEBD is shortly followed by the formation of a bipolar spindle and
102 the alignment of chromosomes at the metaphase plate. The occurrence of peripheral nucleus
103 positioning is correlated with a decreased maturation rate [8]. To assess the meiotic progression,
104 oocytes were collected from mice aged 6-8 weeks and matured for 16 h (Met II). The majority
105 (~92%) of centrally located GV oocytes were able to undergo NEBD. In contrast, peripherally
106 located GV oocytes showed a significant decrease (~61%) in the percentage of NEBD (Figure
107 2A). However, using time-lapse microscopy, we found no significant difference in the timing of
108 NEBD between centrally located GV oocytes and peripherally located GV oocytes (Figure 2B).
109 Similarly, a majority (~81%) of central GV oocytes were able to extrude the first polar body
110 (PBE), while peripheral GV oocytes were less successful in extruding the first polar body
111 (~59%, Fig. 2C). Once again, there was no significant difference in the timing of PBE when both
112 centrally located GV oocytes and peripherally located GV oocytes were compared (Fig. 2D).
113 To assess the chromosome alignment and spindle morphology among groups, oocytes were
114 matured *in vitro* for either 7 h (Met I) or 16 h (Met II), fixed, and immunostained with α-tubulin
115 to label the spindle and stained with DAPI to label DNA. Chromosome alignment was assessed
116 according to the parameters previously described [20]. We found a significant increase in the
117 percentage of chromosome misalignment at both Met I or Met II in oocytes with a more
118 peripherally positioned nucleus when compared to oocytes with a centrally located nucleus.
119 Intermediate GV oocytes also showed significantly higher rates of chromosome misalignment
120 when compared to central GV oocytes at Met I, but not at Met II (Fig. 2E,F,H,I). Spindle
121 morphology was assessed using the criterion that a normal meiotic spindle is barrel shaped with
122 two clearly defined spindle poles. Spindle morphology did not vary significantly among groups
123 either at Met I or Met II (Fig. 2E,G,H,J). Because chromosome misalignment is highly

124 associated with aneuploidy, we then assessed aneuploidy in Met II eggs using *in situ*
125 chromosome counting [21,22]. Strikingly, segregation errors occurred in oocytes with a peripherally
126 located nucleus (~50.15%) approximately 5 times more frequently than in oocytes with a
127 centrally located nucleus (~10.37%, Fig. 2K,L).
128
129 ***Nuclear envelope breakdown occurs during central relocation of peripherally located nucleus***
130 To understand the behavior of the nucleus and its positioning during MI, we employed time-
131 lapse microscopy to image live oocytes. When peripheral GV oocytes were arrested at prophase I
132 (using milrinone, a phosphodiesterase inhibitor) to prevent NEBD, only ~15% of the oocytes
133 remained peripheral within 3 h of incubation, while the majority (~85%) relocated to the center
134 of the oocyte (Supplementary Fig. 2 and Movie 1), confirming that the nucleus favors central
135 movement, as previously reported [9,23,24]. When the oocytes were allowed to mature in milrinone-
136 free medium, nuclei initially located at the periphery of the cell underwent 10 ± 1.256 μm on
137 average of central movement before experiencing NEBD. Intermediately located nucleus and
138 centrally located nucleus underwent central movement and traveled a distance of 6 ± 0.6024 μm
139 and 4 ± 0.6783 μm, respectively, before NEBD (Supplementary Fig. 3A). However,
140 chromosome alignment in oocytes with a peripherally located nucleus remained relatively closer
141 to the oocyte cortex in comparison to chromosome alignment in oocytes with a central nucleus
142 (Supplementary Fig. 3B,C). It is of note that the timing of chromosome alignment did not vary
143 significantly among groups (Supplementary Fig. 3B,D). Why oocytes favor central nucleus
144 positioning is not fully understood.
145

146 ***Incorrect kinetochore-microtubule attachments are increased in oocytes with a peripherally***
147 ***located nucleus***
148 While aneuploidy can occur as a result of many different errors, one important cause of
149 aneuploidy is a weakened or non-functional spindle assembly checkpoint (SAC). Typically, the
150 SAC is inactivated when MTs are attached correctly to all kinetochores, but a weakened or non-
151 functional SAC may allow the progression of the cell to anaphase without proper K-MT
152 attachments, a phenomenon that is highly associated with aneuploidy. To assess the SAC
153 function in oocytes with a central, intermediate, or peripheral nucleus, oocytes were treated with
154 nocodazole, a MT depolymerizing agent that is known to maintain the SAC active and thereby
155 prevent PBE by inducing Met I arrest [22,25]. Expectedly, positive control oocytes treated by
156 ZM447439, an Aurora Kinase B/C inhibitor that is known to disrupt the SAC function at a high
157 dose (10μM), extruded a PB even in the presence of nocodazole [26]. In contrast to ZM447439
158 treated oocytes, all other oocytes (central, intermediate, and peripheral) failed to extrude a PB in
159 the presence of nocodazole, suggesting that the SAC is intact, functional, and therefore not
160 contributing to aneuploidy in peripheral GV oocytes (Supplementary Fig. 4).
161 Improper K-MT attachment is another major contributor of aneuploidy. Because cortically facing
162 centromeres have relatively high rates of unstable K-MT attachments when compared to those
163 away from the oocyte cortex [27] and peripheral nucleus positioning correlates with peripheral
164 spindle assembly (near the cortex), we hypothesized that K-MT attachments are perturbed in
165 peripheral GV oocytes. In meiotic oocytes, even if the SAC is satisfied by present K-MT
166 attachment, it is not necessary that all attachments are correct and homologous chromosomes are
167 bioriented [20,28]. To assess K-MT attachments, Met I oocytes (~7 h) were exposed to a brief cold
168 shock (6 minutes) in order to depolymerize labile unattached MTs and maintain stable MT fibers

169 that are attached to kinetochores. The oocytes were immunostained with α-tubulin (to label
170 MTs), CREST (to label kinetochores), stained with DAPI (to label DNA), and imaged using
171 confocal microscopy. K-MT attachments were scored as normal, unattached, or abnormally
172 attached (merotelic or syntelic) (Fig. 3A). Nucleus positioning had no effect on the percentage of
173 unattached kinetochores among all groups (Fig. 3A,B). Importantly, oocytes with peripherally
174 located nucleus displayed ~ four-fold increase in the percentage of incorrect K-MT attachments,
175 compared to oocytes with a centrally located nucleus (Fig. 3A,C). Moreover, the percentages of
176 peripheral (37.93 ± 9.17%) and intermediate (39.13 ± 10.41%) oocytes having two or more
177 abnormally attached kinetochores were significantly higher than those in the central group (7.14
178 ± 4.02%) (Fig. 3D). These results suggest that improper K-MT attachments are the likely cause,
179 at least in part, of increased aneuploidy in oocytes with a peripherally located nucleus. These
180 results led us to hypothesize that initial spindle formation and its positioning at the oocyte center
181 serves as mechanism to ensure avoidance of cortical influence on the establishment of K-MT
182 attachments, prior to timely spindle migration to the cortex.
183
184 ***Incidence of aneuploidy directly associated with the proximity of early spindle positioning to***
185 ***the cortex***
186 To confirm that the cortical influence during spindle formation is the cause, at least partially, of
187 the high rate of aneuploidy in peripheral GV oocytes, we tracked the movement of the nucleus
188 using live time-lapse microscopy. Oocytes with a peripherally located nucleus demonstrated one
189 of three types of movement: oocytes that were able to achieve complete relocation of the nucleus
190 to the center prior to NEBD were termed 'corrected', oocytes that demonstrated central
191 movement prior to NEBD but did not achieve full relocation were termed 'migratory', and

192 oocytes that failed to make a relocation attempt and remained at the cortex through NEBD were
193 termed 'peripheral' (Fig. 4A,B and supplementary movies 2-4). Strikingly, oocytes that were
194 able to successfully relocate their nucleus to the center showed relatively lower rates of
195 aneuploidy (comparable to that of oocytes beginning with a central nucleus) when compared to
196 oocytes that failed nucleus relocation and underwent NEBD at the periphery of the oocyte (Fig.
197 4C).
198 It is technically feasible to shift the position of the spindle within the oocyte without noticeable
199 adverse effects [29,30]. Therefore, to further confirm the relationship between aneuploidy and the
200 proximity of early spindle positioning to the cortex, we relocated the spindle prematurely to the
201 cortex through mild centrifugation, a technique proven successful in murine oocytes (Fig. 4D) [31].
202 Central GV oocytes were matured *in vitro* for 4 h, until prometaphase (the time prior to
203 establishing correct K-MT attachments [32]). These prometaphase oocytes were centrifuged,
204 examined live under the microscope and resorted into two groups according to their spindle
205 positioning: those maintaining central positioning (control central) and those with induced
206 peripheral positioning (induced peripheral) prior to *in vitro* maturation for an additional 13 h
207 (Met II). Notably, oocytes with induced peripheral positioning showed significantly higher rates
208 of aneuploidy (58.33%) when compared to oocytes maintaining central spindle positioning after
209 centrifugation (16.67%, Fig. 4E); thus suggesting that peripheral GV oocytes are not inherently
210 erroneous, but instead are subjected to increased levels of cortical influence that is detrimental to
211 the fidelity of chromosome segregation.
212
213 ***Inhibition of the Cdc42 cortical gradient permits normal formation of K-MT attachment in***
214 ***oocytes with peripheral spindle formation***

215 Recent study showed that Cdc42 signals coming from the oocyte cortex can influence K-MT
216 attachments through tyrosination of MTs close to the cortex [27]. In mitotic cells, tyrosinated MTs
217 are associated with abnormal K-MT attachments [33]. From these findings, we hypothesized that
218 premature exposure to increased cortical Cdc42 signals in oocytes with a peripherally positioned
219 spindle during prometaphase could hinder the oocyte's ability to establish and/or stabilize correct
220 K-MT attachments. To this end, oocytes were matured *in vitro* for 5 h. Based on spindle position
221 using live imaging, oocytes were sorted into two groups: central and peripheral oocytes. At this
222 point, the treatment groups were supplemented with a Cdc42 inhibitor (ML141), whereas control
223 oocytes were supplemented with dimethyl sulfoxide (DMSO) for an additional 2 h (Fig. 4F). Met
224 I oocytes were exposed to a 6 minutes cold shock followed by the assessment of K-MT
225 attachments using immunocytochemistry and confocal microscopy. K-MT attachments were
226 scored as normal, unattached, or abnormally attached (merotelic or syntelic). The number of
227 unattached kinetochores did not differ significantly among groups (Fig. 4G). Expectedly, oocytes
228 with peripherally positioned spindles (during prometaphase I) exhibited a significant increase in
229 the percentage of abnormal K-MT attachments, compared to those with a centrally positioned
230 spindle. Importantly, inhibition of cortical Cdc42 signals using ML141 rescued, at least in part,
231 the percentage of abnormal K-MT attachments in non-treated oocytes with a peripherally
232 positioned spindle (Fig. 4H). These results suggest that avoidance of the cortical cdc42 signals
233 during prometaphase I is critical in protecting the oocyte's ability to establish correct K-MT
234 attachments and further undergo faithful chromosome segregation (Fig. 5).
235

236 **DISCUSSION**

237 Most errors contributing to aneuploid embryos occur in female gametes, specifically within the
238 first meiotic division [5,6]; therefore, it is crucial to understand the tightly regulated mechanisms
239 that ensure faithful chromosome segregation. Our findings suggest that central nucleus
240 positioning serves as a preemptive insurance mechanism to ensure that the spindle forms at the
241 center of the oocyte and avoids deleterious cortical Cdc42 signals. These cortical signals are
242 capable of affecting the fidelity of proper K-MT attachment formation. Indeed, when the spindle
243 is prematurely exposed to cortical signals, due to peripheral nucleus positioning or premature
244 induction of cortical positioning of the spindle, the oocyte experiences significantly increased
245 levels of abnormal K-MT attachment and aneuploidy.
246
247 Abnormal K-MT attachments during Met I is a major cause of aneuploidy in mammalian oocytes
248 [22,34,35]. Our results showed that peripheral GV oocytes that displayed a correction mechanism by
249 relocating their nuclei to the center (before spindle assembly) displayed a significant decrease in
250 the percentage of abnormal K-MT attachments when compared to uncorrected oocytes,
251 suggesting that the cortical signals may have an influence on the ability of the oocyte to establish
252 correct K-MT attachments. In mitotic cells, tyrosinated MTs form early K-MT attachments, but
253 correctly established attachments become detyrosinated and stabilize as spindle tension
254 increases. Incorrect attachments remain tyrosinated (unstable) and are thus more likely to
255 depolymerize [33].In addition, recent evidence suggests that cortical Cdc42 signals have the
256 capability to influence K-MT attachments and centromeric selection in meiotic oocytes through
257 spindle asymmetry and MT tyrosination. Consistently, we found that inhibition of Cdc42 largely
258 rescued increased abnormal K-MT attachments in peripherally assembled and positioned spindle.
259 Taken together, our results suggest that primary spindle formation and positioning at the center

260 of the oocyte may serve as an essential protection mechanism against cortical signals capable of
261 influencing improper K-MT attachments.
262
263 Nucleus positioning in meiotic oocytes is often studied only *in vitro* or at a single time point *in*
264 *vivo* and is thus not well understood. There has been a long-standing debate regarding the
265 position of the nucleus in mammalian oocytes. For example, a previous study found that the
266 majority of prophase I-arrested oocytes have a peripherally located nucleus, and this cortical
267 positioning of the nucleus is likely influenced by gap junctions and increased cumulus cell
268 contact [36]. On the other hand, other studies demonstrated that the majority of prophase I-arrested
269 oocytes have a centrally positioned nucleus [8,37,38]. Interestingly, in the first study [36], the oocytes
270 were collected from mice aged 21 days, whereas in the other studies [8,37,38], the oocytes were
271 collected from mice aged more than 6-8-week old. Our results– that the majority of oocytes
272 collected from 2-3-week old mice exhibited a peripherally located nucleus, whereas the majority
273 of oocytes from 6-8-week old mice exhibited a centrally located nucleus– clearly explain these
274 previous findings and advance our understanding of an important phenomenon in mammalian
275 oocytes.
276
277 Although the nucleus shifts from a peripheral position in prepubertal oocytes towards a central
278 position in sexually mature mouse oocytes, this is likely not the only shift during the
279 reproductive life. Indeed, oocytes from aged mice have a majority of peripherally positioned
280 nuclei [8]. Why and how nucleus positioning is a dynamic process during oocyte development
281 remains unknown. It is unlikely that age-dependent nucleus positioning is due to the difference
282 in the response to gonadotropins because FSHβ knockout mice showed similar proportions of

283 central *vs.* peripheral GV oocytes to those of WT mice (Kincade, J., Almamun, Marshall, K., M.,
284 Rivera, R. and Balboula, A., unpublished data). During oocyte meiosis, prophase I-arrested
285 oocytes have a cytoplasmic mesh of F-actin-coated vesicles that experience increased movement
286 near the cortex and decreased movement near the center. Accordingly, the gradient of F-actin
287 creates a gentle force that encourages the nucleus to position at the center of the cell through
288 active diffusion [9,10]. Analyzing the cytoskeletal changes within the oocyte during its development
289 and growth may reveal more insight into the underlying mechanisms behind nucleus positioning
290 throughout oogenesis.
291
292 Current *in vitro* fertilization (IVF) technologies maintain much room for improvement, as only
293 12.7% of naturally ovulated IVF cycles in humans produce a pregnancy and only 8.8% of those
294 pregnancies result in live births [39]. Although technologies and protocols have advanced since the
295 first IVF birth in 1978, the success rate in producing a live birth in women under the age of 35
296 through IVF remains less than 50% [40]. To date, there are no definitive morphological markers of
297 predictive oocyte quality and successful IVF that are particularly non-invasive [41]. Gametes from
298 human females are notoriously associated with high rates of aneuploidy [5,42]. In addition, human
299 oocytes with a peripherally located nucleus are associated with poor maturation rates compared
300 to those with a centrally located nucleus [37]. Therefore, understanding the association between
301 peripherally located nucleus and the incidence of aneuploidy may allow for the selection of
302 oocytes predisposed to correct segregation of chromosomes. Additionally, arresting the cell and
303 enabling the nucleus to relocate to central positioning may be a promising approach to increase
304 the overall efficacy of IVF practices, allowing for increases in blastocyst rate, pregnancy rate,
305 and live birth rate in all species.

306

307 # MATERIAL AND METHODS

308 ***Ethics***

309 All laboratory animals were managed, and experiments conducted, in compliance with the
310 University of Missouri (Animal Care Quality Assurance Reference Number, 9695).

311

312 ***Mouse strains***

313 Unless otherwise specified, female CF-1 WT mice were used. *Cep192-eGfp* reporter mice were
314 generated by integrating a construct harboring the EGFP reporter gene into CF-1 mouse genome
315 via CRISPR/Cas9-mediated homology-directed repair. The EGFP reporter was fused at the C-
316 terminus of the endogenous mouse Cep192. Homozygous breeding pairs of *Cep192-eGfp*
317 reporter mice were used to maintain the colony.

318

319 ***Oocyte collection and in vitro maturation (IVM)***

320 Full-grown GV oocytes were collected from CF-1 female mice (not primed by pregnant mare
321 serum gonadotropin) aged 6-8 weeks. Oocyte collection and culture were carried out as
322 previously described [22,43]. Cumulus oocyte complexes (COCs) were collected and cultured in
323 bicarbonate-free minimal essential medium (MEM) supplemented with 3mg/ml
324 polyvinylpyrrolidone (PVP) and 25 mM Hepes (pH 7.3) under mineral oil (MilliporeSigma, St.
325 Louis, MO, USA # M4659, # P2307, # H3784, # M8410). Oocytes were manually denuded and
326 sorted into 3 groups: Central GV, Intermediate GV, Peripheral GV oocytes. Careful rolling of the
327 oocyte ensured correct classification. Oocytes were then transferred to Chatot, Ziomek, and

328 Bavister (CZB) medium [44] supplemented with 1µM glutamine (MilliporeSigma, # G8549) under
329 mineral oil and matured at 37˚C with humidified 5% CO_2 in an incubator for either 7, 14, or 16 h.
330 Nocodazole (Sigma #M1404), monastrol (Sigma #M8515), ML141 (Sigma #SML0407)and
331 ZM447439 (Tocris #2458) were dissolved in DMSO and added to CZB culture medium at a final
332 concentration of 5 µm, 100 µM, 500 nM and 10 µm, respectively. SiR-tubulin and SiR-DNA
333 were added to the maturation medium (at a final concentration of 100 nM) during live imaging to
334 label MTs and DNA, respectively.
335
336 ***Immunocytochemistry***
337 After maturation, oocytes were fixed in a freshly prepared solution of 3.7% paraformaldehyde
338 (MilliporeSigma, # P6148) dissolved in phosphate buffer saline (PBS). Oocytes were incubated
339 in permeabilization solution (0.1% Triton X-100 in PBS) for 20 minutes and blocking solution
340 (0.3% BSA and 0.01% Tween-20 in PBS) for 20 minutes before staining. Oocytes were
341 incubated at room temperature for one h with the primary antibody before undergoing 3
342 consecutive washes in blocking solution for 9 minutes each. Oocytes were then incubated at
343 room temperature for one h in the secondary antibody solution. Following another 3 consecutive
344 washes in blocking solution at 9 minutes each, oocytes were mounted on glass slides using
345 Vectashield containing 4',6-Diamidino-2-Phenylindole, Dihydrochloride (DAPI; Vector
346 Laboratories, Burlingame, CA, USA) in order to stain the DNA. Fluorescence was observed
347 using a 40X oil objective using Leica TCS SP8 confocal microscope or Leica DMI8 fluorescence
348 microscope and oocytes were imaged using 3 µm Z-intervals. Oocytes were analyzed using NIH
349 ImageJ software (National Institute of Health, Bethesda, MD USA).

350 The following primary antibodies were used in immunofluorescence: conjugated α-tubulin-
351 AlexaFluor 488 (Life Technologies # 322 588; 1:75), CREST autoimmune serum (Antibodies
352 Incorporated # 15-234; 1:25).
353
354 ***In situ chromosome counting***
355 Oocytes matured *in vitro* for 14 h in CZB medium supplemented with L-glutamine under mineral
356 oil were transferred to CZB containing 100 µm monastrol (MilliporeSigma, # M8515) and
357 incubated an extra 2 h; monastrol is an Eg5-kinesin inhibitor which induces monopolar spindle
358 formation and thus results in a rosette of chromosome distribution [21,22]. After treatment with
359 monastrol, oocytes at Met II stage were fixed in a freshly prepared solution of 2.5%
360 paraformaldehyde (MilliporeSigma, # P6148) and stained with CREST autoimmune serum
361 (Antibodies Incorporated # 15-234; 1:25) to label the kinetochores. DAPI was used to label the
362 DNA. Fluorescence was observed using a 40X oil objective using a Leica DMI8 microscope and
363 oocytes were imaged using 0.5 µm Z-intervals in order to observe all kinetochores. Oocytes were
364 analyzed individually and were scored either as euploid (containing 40 kinetochores) or as
365 aneuploid (containing ± 40 kinetochores).
366
367 ***Assessment of kinetochore-microtubule attachment***
368 Cells were matured *in vitro* for 7 h in CZB medium supplemented with L-glutamine under
369 mineral oil. The oocytes were placed on ice for 6 minutes in a 96 well dish containing chilled
370 MEM. Exposing the oocytes to cold shock depolymerizes unattached MTs; however, when MTs
371 have established end-on attachment to a kinetochore, it becomes cold stable [45]. Oocytes were
372 fixed using a freshly prepared 2.5% paraformaldehyde solution and immunostained with anti-

373 human CREST (to label kinetochores) and α-tubulin (to label MTs) antibodies. DAPI was used
374 to label DNA. Cells were imaged using a Leica TCS SP8 confocal microscope and a x63 oil
375 objective, taking images at 0.5 µm Z-intervals. Kinetochores were analyzed for unattached,
376 normal, or abnormal attachments (syntelic - both kinetochores attached to one side of the spindle
377 or merotelic - a kinetochore maintaining attachment to both sides of the spindle). Oocytes were
378 analyzed using NIH ImageJ Software.
379
380 ***Time-lapse microscopy***
381 Full-grown oocytes were imaged using a 40X oil objective on Leica TCS SP8 confocal
382 microscope or Leica DMI8 microscope within a microenvironmental chamber maintaining an
383 atmosphere of 5% CO_2 and temperature of 37˚C in humidified air. Imaging acquisition began
384 before NEBD. Images were captured at 5 µm Z-intervals. Image sequences were analyzed using
385 NIH ImageJ Software.
386
387 ***Ovary collection and histological evaluation***
388 Ovaries from CF-1 mice of varying ages (2 weeks, 3 weeks, 5 weeks, and 8 weeks) were
389 collected, submerged, and stored in buffered zinc formalin overnight. Tissues were then moved
390 to 70% ethanol for storage until undergoing a 10-h protocol using a Leica ASP300S enclosed
391 tissue processor. After processing, tissues were embedded in paraffin wax and cooled fully using
392 the Leica EG1150 C/H pair. Embedded tissues were sectioned at 8 µm thickness using a Leica
393 Histocore AutoCut microtome. Representative samples were taken for each age by taking 3
394 consecutive sections periodically (every 4, 6, 8, or 10 sections respectively). Tissues were
395 stained with Hematoxylin and Eosin (Abcam, # 245880) before being mounted with permount

resin (Thermo Fisher Scientific, Inc. # SP15). Oocytes and their corresponding nucleus positioning were examined using 10X or 40X objective on a Leica DMI8 microscope.

Statistical analysis

Tests used to evaluate the statistical significance of the findings reported include One-way ANOVA and Student t-test using GraphPad Prism. The Tukey post hoc test was utilized to determine statistical significance between groups. P values of < 0.05 were considered significant. All data are displayed as means ± SEM.

Declaration of interest

All authors declare that there are no conflicts of interest that may prejudice or bias the research reported.

Funding

This research was supported by laboratory start-up funding from the University of Missouri to AZB.

Acknowledgements

The authors would like to thank all members of the Balboula lab at the University of Missouri, Columbia for dedicated help and encouragement. The authors would like to thank Rocio Rivera, Heide Schatten for critical reading of the manuscript and valuable discussion, and Yuksel Agca, Pramod Dhakal, Thomas Spencer, the Animal Modeling Core and the Molecular Cytology Core for equipment usage and valuable discussion.

Author Contributions

AZB conceived the project. AZB and JK designed and analyzed experiments. JK performed experiments. AZB and JK wrote the manuscript.

Figure Legends

Figure 1: Nucleus positioning is a dynamic process throughout the development

(A) Full-grown GV oocytes were collected, imaged and classified into one of three groups: central GV, intermediate GV, or peripheral GV according to the distance measured from the nucleus to the nearest cortex. The scale bar represents 50 µm. Quantification of the average distance from the nucleus to the nearest cortex within groups (right graph). One-way ANOVA and Tukey's post hoc test were performed to analyze the data. (B) Representative images of oocytes with a central, intermediate, and peripherally located nucleus. The scale bars represent 100 µm. Quantification of the contribution of each group to all oocytes collected (right graph). One-way ANOVA and Tukey's post hoc test were performed to analyze the data. (C) Histological analysis of nucleus positioning *in vivo* at different ages. Ovaries from 2, 3, 5, and 8 weeks old mice were collected, fixed, and stained with Hematoxylin and Eosin. Sections were observed through 10X and 40X objective magnification and classified into one of the three positioning groups: central, intermediate, peripheral. The scale bar represents 100 µm. (D) Representative images of nucleus positioning in 3 and 8 weeks old mice. The white box emphasizes the location of the magnified image within the ovary. The scale bar represents 100 µm. (E) Quantification of the proportion of oocytes sorted according to their nucleus positioning (central, intermediate, peripheral) in 2, 3, 5, and 8 week old mice. Two-way ANOVA and Sidak's multiple comparison test were performed to determine if the groups differed

442 significantly. Data are displayed as mean ± SEM. Values with asterisks vary significantly, * P
443 <0.05, ** P <0.01, *** P <0.001, **** P <0.0001. The total number of analyzed oocytes (from 3
444 independent replicates) is specified above each graph.
445
446 **Figure 2: Oocytes with a peripherally located nucleus have higher rates of chromosome**
447 **misalignment and aneuploidy.**
448 Full-grown prophase I-arrested oocytes were collected and sorted into central, intermediate and
449 peripheral groups based on nucleus positioning and imaged live using time-lapse microscopy
450 during *in vitro* maturation. (A) Quantification of the percentage of oocytes that underwent
451 NEBD. (B) Quantification of the average time of NEBD. (C) Quantification of the percentage of
452 first polar body extrusion (1st PBE). (D) Quantification of the average time of PBE calculated
453 from oocytes successfully extruded the PB. (E-J) Full-grown prophase I oocytes were collected
454 and sorted into central, intermediate and peripheral groups based on nucleus positioning and *in*
455 *vitro* matured for 7 h (Met I) or 16 h (Met II. Oocytes were fixed and immunostained with α-
456 tubulin to label the microtubules (the spindle). DNA was labeled by DAPI. (E) Representative
457 confocal images of Met I oocytes. (F) Quantification of the percentage of chromosome
458 misalignment in Met I oocytes. (G) Quantification of the percentage of abnormal spindle
459 morphology in Met I oocytes. (H) Representative confocal images of Met II oocytes. (I)
460 Quantification of the percentage of chromosome misalignment in Met II oocytes. (J)
461 Quantification of the percentage of abnormal spindle morphology in Met II oocytes. (K) Full-
462 grown prophase I oocytes were collected and sorted into central, intermediate and peripheral
463 groups based on nucleus positioning and *in vitro* matured for 14 h (Met II). Oocytes were treated
464 with monastrol for 2 h, fixed and immunostained with CREST antibody to label kinetochores.

465 DNA was labeled by DAPI. Oocytes were analyzed individually and scored either as euploid
466 (containing 40 kinetochores) or as aneuploid (containing ± 40 kinetochores). Shown are
467 representative images. (L) Quantification of the percentage of aneuploid eggs. The scale bar
468 represents 10 µm. One-way ANOVA and Tukey's post hoc tests were performed to determine
469 statistical significance among groups. Data are displayed as mean ± SEM. Values with asterisks
470 vary significantly, * P <0.05, *** P <0.001, **** P <0.0001. The total number of analyzed
471 oocytes (from at least 3 independent replicates) is specified above each graph.
472
473 **Figure 3: Oocytes with peripherally located nucleus experience higher levels of incorrect**
474 **kinetochore-microtubule attachments**
475 (A) Representative images of kinetochore-microtubule (K-MT) attachments in oocytes with a
476 central, intermediate, or peripherally located nucleus. Panels on the right (from top to bottom)
477 display normal K-MT attachment, unattached kinetochores and abnormal K-MT attachment. (B)
478 Quantification of the percentage of unattached kinetochores and (C) abnormal K-MT
479 attachments. (D) Quantification of the oocytes with 2 or more incorrect K-MT attachments. One-
480 way ANOVA and Tukey's post hoc test were performed to analyze the data. Data are displayed
481 as mean ± SEM. Values with asterisks vary significantly, * P <0.05, ** P <0.01, **** P <0.0001.
482 The total number of analyzed oocytes (from 4 independent replicates) is specified above each
483 graph.
484
485 **Figure 4: Incidence of incorrect K-MT attachments and aneuploidy associate with spindle**
486 **proximity to the cortex**

487 (A) Schematic depicting the determination of corrected, migratory, and peripheral oocytes. (B)
488 Representative images of the nucleus movement prior to NEBD. Images were taken every 30
489 minutes (Z-interval of 5 µm). The black circle denotes the primary nucleus positioning, while the
490 green circle denotes the final nucleus position prior to NEBD. (C) Quantification of the
491 incidence of aneuploidy in metaphase II oocytes from the oocytes categorized in B. One-way
492 ANOVA and Tukey's post hoc test were performed to determine statistical significance. (D)
493 Schematic depicting the induction of peripheral spindle positioning by mild centrifugation in
494 oocytes collected with a centrally positioned nucleus. (E) Quantification of the incidence of
495 aneuploidy in oocytes with induced peripherally positioned nucleus and centrally positioned
496 nucleus after centrifugation. Student t-test was performed to determine statistical significance.
497 Data are displayed as mean ± SEM. Values with asterisks vary significantly, * $P < 0.05$. (F)
498 Schematic depicting the treatment of collected oocytes with ML141, a Cdc42 inhibitor, in order
499 to inhibit the cortical influence upon kinetochore-microtubule (K-MT) attachment formation.
500 (G,H) Quantification of the average incidence of unattached kinetochores and abnormal K-MT
501 attachment, respectively. One-way ANOVA and Tukey's post hoc test were performed to
502 determine statistical significance. Data are displayed as mean ± SEM. Values with asterisks vary
503 significantly, * $P < 0.05$, ** $P < 0.01$. The total number of analyzed oocytes (from 3 independent
504 replicates) is specified above each graph.
505
506 **Figure 5:** A summary schematic depicting the deleterious influence of cortical Cdc42 upon
507 proper K-MT attachments in oocytes with a peripherally positioned spindle that is at least
508 partially contributory to the development of aneuploid gametes. The lower section of the

509 schematic demonstrates the ability of the oocyte to establish correct K-MT attachments in
510 oocytes with a centrally positioned spindle and thus avoid chromosome mis-segregation.
511
512 **Supplementary Figure 1:** Full-grown prophase I-arrested oocytes were collected from *Cep192-*
513 *eGfp* reporter mice, sorted into central (A) and peripheral (B) groups based on the positioning of
514 their nucleus and *in vitro* matured in CZB medium containing SiR-tubulin (to label microtubules,
515 magenta). Spindle poles were labeled by CEP192-EGFP (MT organizing centers, green).
516 Oocytes were imaged live using time-lapse confocal microscopy. Shown are representative
517 fluorescence and bright-field (lower panels) image sequence depicting the location of NEBD and
518 consequent spindle formation. Images were taken every 1 h (Z-projection of 13 sections every 5
519 µm). The scale bar represents 50 µm.
520
521 **Supplementary Figure 2:** (A) Representative bright-field images of time-lapse microscopy of
522 the movement of a peripherally positioned nucleus during prophase I arrest in oocytes incubated
523 with milrinone. Images were taken every 10 minutes using a Z-interval of 5 µm. The black circle
524 identifies the initial positioning of the nucleus, while the green circle denotes the final
525 positioning of the nucleus immediately prior to NEBD. (B) Quantification of the percentage of
526 peripheral and intermediate GV oocytes achieving full relocation of the nucleus to a central
527 position within 3 h of incubation with milrinone.
528
529 **Supplementary Figure 3:** Full-grown prophase I-arrested oocytes were collected and sorted into
530 central, intermediate, and peripheral groups based on the positioning of their nucleus and imaged
531 live using time-lapse microscopy during *in vitro* maturation. (A) Quantification of the change in

532 the distance of the nucleus to the nearest cortex from the initial position of the nucleus at the
533 prophase I-arrested stage to the final destination of the nucleus immediately prior to NEBD. (B)
534 Representative fluorescence and bright-filed (lower panels) image sequence depicting
535 chromosome alignment (labeled by SiR-DNA, red) in oocytes with a central (upper) and
536 peripheral (lower) nucleus. Images were taken every 45 minutes using a Z-interval of 7 μm.
537 Scale bars represent 50 μm. (C) Quantification of the distance of chromosomes at the time of
538 alignment to the nearest cortex. (D) Quantification of the time of chromosome alignment. One-
539 way ANOVA and Tukey's post hoc test were performed to determine statistical significance.
540 Data are displayed as mean ± SEM. Values with asterisks vary significantly, ** P <0.01, *** P
541 <0.001. The total number of analyzed oocytes (from 3 independent replicates) is specified above
542 each graph.
543
544 **Supplementary Figure 4:** (A) Full-grown prophase I-arrested oocytes were collected, sorted
545 (into central, intermediate, and peripheral groups based on the positioning of their nucleus) and
546 *in vitro* matured in the presence of nocodazole. Randomly selected oocytes were *in vitro* matured
547 in the presence of nocodazole and ZM447439 (positive control group). The percentage of first
548 polar body extrusion (PBE) was assessed at 16 h (Met II). One-way ANOVA and Tukey's post
549 hoc test were performed to determine statistical significance. Data are displayed as mean ± SEM.
550 Values with asterisks vary significantly, **** P <0.0001. The total number of analyzed oocytes
551 (from 4 independent replicates) is specified above the graph.
552

553 **Supplementary Movie 1:** Time-lapse microscopy of germinal vesicle (GV) oocytes cultured in
554 milrinone-containing medium to maintain prophase I arrest. DIC images were captured every 10
555 minutes at Z-intervals of 5 µm. The scale bar represents 50 µm.
556
557 **Supplementary Movie 2:** Time-lapse microscopy of peripheral germinal vesicle (GV) oocyte
558 showing corrected nucleus relocation during *in vitro* maturation (Same oocyte used in the top
559 panels of Fig. 4B). DIC images were captured every 10 minutes at Z-intervals of 5 µm. The scale
560 bar represents 50 µm.
561
562 **Supplementary Movie 3:** Time-lapse microscopy of peripheral germinal vesicle (GV) oocyte
563 showing migratory nucleus relocation during *in vitro* maturation (Same oocyte used in the
564 middle panels of Fig. 4B). DIC images were captured every 10 minutes at Z-intervals of 5 µm.
565 The scale bar represents 50 µm.
566
567 **Supplementary Movie 4:** Time-lapse microscopy of peripheral germinal vesicle (GV) oocyte
568 that failed to relocate its nucleus during *in vitro* maturation (Same oocyte used in the lower
569 panels of Fig. 4B). DIC images were captured every 10 minutes at Z-intervals of 5 µm. The scale
570 bar represents 50 µm.
571

572 **REFERENCES**

573 1 Sun, H. *et al.* Global, regional, and national prevalence and disability-adjusted life-years
574 for infertility in 195 countries and territories, 1990-2017: results from a global burden of
575 disease study, 2017. *Aging (Albany NY)* **11**, 10952-10991, doi:10.18632/aging.102497
576 (2019).
577 2 Jacobs, P. A., Baikie, A. G., Court Brown, W. M. & Strong, J. A. The somatic
578 chromosomes in mongolism. *Lancet* **1**, 710, doi:10.1016/s0140-6736(59)91892-6 (1959).
579 3 Lejeune, J., Turpin, R. & Gautier, M. [Mongolism; a chromosomal disease (trisomy)].
580 *Bull Acad Natl Med* **143**, 256-265 (1959).
581 4 Gruhn, J. R. *et al.* Chromosome errors in human eggs shape natural fertility over
582 reproductive life span. *Science* **365**, 1466-1469, doi:10.1126/science.aav7321 (2019).
583 5 Hassold, T., Hall, H. & Hunt, P. The origin of human aneuploidy: where we have been,
584 where we are going. *Hum Mol Genet* **16 Spec No. 2**, R203-208,
585 doi:10.1093/hmg/ddm243 (2007).
586 6 Hall, H. E. *et al.* The origin of trisomy 22: evidence for acrocentric chromosome-specific
587 patterns of nondisjunction. *Am J Med Genet A* **143A**, 2249-2255,
588 doi:10.1002/ajmg.a.31918 (2007).
589 7 Gilbert, S. in *Developmental Biology* Vol. 6th edition (Sinauer Associates, Inc, 2000).
590 8 Brunet, S. & Maro, B. Germinal vesicle position and meiotic maturation in mouse oocyte.
591 *Reproduction* **133**, 1069-1072, doi:10.1530/REP-07-0036 (2007).
592 9 Almonacid, M. *et al.* Active diffusion positions the nucleus in mouse oocytes. *Nat Cell*
593 *Biol* **17**, 470-479, doi:10.1038/ncb3131 (2015).
594 10 Almonacid, M., Terret, M. E. & Verlhac, M. H. Control of nucleus positioning in mouse
595 oocytes. *Semin Cell Dev Biol* **82**, 34-40, doi:10.1016/j.semcdb.2017.08.010 (2018).
596 11 Colin, A. *et al.* Active diffusion in oocytes nonspecifically centers large objects during
597 prophase I and meiosis I. *J Cell Biol* **219**, doi:10.1083/jcb.201908195 (2020).
598 12 Schuh, M. & Ellenberg, J. Self-organization of MTOCs replaces centrosome function
599 during acentrosomal spindle assembly in live mouse oocytes. *Cell* **130**, 484-498,
600 doi:10.1016/j.cell.2007.06.025 (2007).
601 13 Clift, D. & Schuh, M. A three-step MTOC fragmentation mechanism facilitates bipolar
602 spindle assembly in mouse oocytes. *Nat Commun* **6**, 7217, doi:10.1038/ncomms8217
603 (2015).
604 14 Balboula, A. Z. *et al.* Haspin kinase regulates microtubule-organizing center clustering
605 and stability through Aurora kinase C in mouse oocytes. *J Cell Sci* **129**, 3648-3660,
606 doi:10.1242/jcs.189340 (2016).
607 15 Luksza, M., Queguigner, I., Verlhac, M. H. & Brunet, S. Rebuilding MTOCs upon
608 centriole loss during mouse oogenesis. *Dev Biol* **382**, 48-56,
609 doi:10.1016/j.ydbio.2013.07.029 (2013).
610 16 McCarthy, E. K. & Goldstein, B. Asymmetric spindle positioning. *Curr Opin Cell Biol*
611 **18**, 79-85, doi:10.1016/j.ceb.2005.12.006 (2006).
612 17 Longo, F. J. & Chen, D. Y. Development of cortical polarity in mouse eggs: involvement
613 of the meiotic apparatus. *Dev Biol* **107**, 382-394 (1985).
614 18 Ma, J., Zeng, F., Schultz, R. M. & Tseng, H. Basonuclin: a novel mammalian maternal-
615 effect gene. *Development* **133**, 2053-2062, doi:10.1242/dev.02371 (2006).

616 19 Menezo, Y. J. Paternal and maternal factors in preimplantation embryogenesis:
617 interaction with the biochemical environment. *Reprod Biomed Online* **12**, 616-621,
618 doi:10.1016/s1472-6483(10)61188-1 (2006).
619 20 Lane, S. I., Yun, Y. & Jones, K. T. Timing of anaphase-promoting complex activation in
620 mouse oocytes is predicted by microtubule-kinetochore attachment but not by bivalent
621 alignment or tension. *Development* **139**, 1947-1955, doi:10.1242/dev.077040 (2012).
622 21 Duncan, F. E., Chiang, T., Schultz, R. M. & Lampson, M. A. Evidence that a defective
623 spindle assembly checkpoint is not the primary cause of maternal age-associated
624 aneuploidy in mouse eggs. *Biol Reprod* **81**, 768-776, doi:10.1095/biolreprod.109.077909
625 (2009).
626 22 Balboula, A. Z. & Schindler, K. Selective disruption of aurora C kinase reveals distinct
627 functions from aurora B kinase during meiosis in mouse oocytes. *PLoS Genet* **10**,
628 e1004194, doi:10.1371/journal.pgen.1004194 (2014).
629 23 Sanfins, A., Lee, G. Y., Plancha, C. E., Overstrom, E. W. & Albertini, D. F. Distinctions
630 in meiotic spindle structure and assembly during in vitro and in vivo maturation of mouse
631 oocytes. *Biol Reprod* **69**, 2059-2067, doi:10.1095/biolreprod.103.020537 (2003).
632 24 Sanfins, A., Plancha, C. E., Overstrom, E. W. & Albertini, D. F. Meiotic spindle
633 morphogenesis in in vivo and in vitro matured mouse oocytes: insights into the
634 relationship between nuclear and cytoplasmic quality. *Hum Reprod* **19**, 2889-2899,
635 doi:10.1093/humrep/deh528 (2004).
636 25 Balboula, A. Z., Schindler, K., Kotani, T., Kawahara, M. & Takahashi, M. Vitrification-
637 induced activation of lysosomal cathepsin B perturbs spindle assembly checkpoint
638 function in mouse oocytes. *Mol Hum Reprod* **26**, 689-701, doi:10.1093/molehr/gaaa051
639 (2020).
640 26 Lane, S. I., Chang, H. Y., Jennings, P. C. & Jones, K. T. The Aurora kinase inhibitor
641 ZM447439 accelerates first meiosis in mouse oocytes by overriding the spindle assembly
642 checkpoint. *Reproduction* **140**, 521-530, doi:10.1530/REP-10-0223 (2010).
643 27 Akera, T. *et al.* Spindle asymmetry drives non-Mendelian chromosome segregation.
644 *Science* **358**, 668-672, doi:10.1126/science.aan0092 (2017).
645 28 Sebestova, J., Danylevska, A., Novakova, L., Kubelka, M. & Anger, M. Lack of response
646 to unaligned chromosomes in mammalian female gametes. *Cell Cycle* **11**, 3011-3018,
647 doi:10.4161/cc.21398 (2012).
648 29 Schuh, M. & Ellenberg, J. A new model for asymmetric spindle positioning in mouse
649 oocytes. *Curr Biol* **18**, 1986-1992, doi:10.1016/j.cub.2008.11.022 (2008).
650 30 Tatham, B. G. *et al.* Centrifugation of bovine oocytes for nuclear micromanipulation and
651 sperm microinjection. *Hum Reprod* **11**, 1499-1503,
652 doi:10.1093/oxfordjournals.humrep.a019425 (1996).
653 31 Metchat, A. *et al.* An actin-dependent spindle position checkpoint ensures the asymmetric
654 division in mouse oocytes. *Nat Commun* **6**, 7784 (retracted), doi:10.1038/ncomms8784
655 (2015).
656 32 Kitajima, T. S., Ohsugi, M. & Ellenberg, J. Complete kinetochore tracking reveals error-
657 prone homologous chromosome biorientation in mammalian oocytes. *Cell* **146**, 568-581,
658 doi:10.1016/j.cell.2011.07.031 (2011).
659 33 Ferreira, L. T. *et al.* alpha-Tubulin detyrosination impairs mitotic error correction by
660 suppressing MCAK centromeric activity. *J Cell Biol* **219**, doi:10.1083/jcb.201910064
661 (2020).

662 34 Orr, B., Godek, K. M. & Compton, D. Aneuploidy. *Curr Biol* **25**, R538-542,
663 doi:10.1016/j.cub.2015.05.010 (2015).
664 35 Lane, M., Bavister, B. D., Lyons, E. A. & Forest, K. T. Containerless vitrification of
665 mammalian oocytes and embryos. *Nat Biotechnol* **17**, 1234-1236, doi:10.1038/70795
666 (1999).
667 36 Barrett, S. L. & Albertini, D. F. Cumulus cell contact during oocyte maturation in mice
668 regulates meiotic spindle positioning and enhances developmental competence. *J Assist*
669 *Reprod Genet* **27**, 29-39, doi:10.1007/s10815-009-9376-9 (2010).
670 37 Levi, M., Ghetler, Y., Shulman, A. & Shalgi, R. Morphological and molecular markers
671 are correlated with maturation-competence of human oocytes. *Hum Reprod* **28**, 2482-
672 2489, doi:10.1093/humrep/det261 (2013).
673 38 Almonacid, M. *et al.* Active Fluctuations of the Nuclear Envelope Shape the
674 Transcriptional Dynamics in Oocytes. *Dev Cell* **51**, 145-157 e110,
675 doi:10.1016/j.devcel.2019.09.010 (2019).
676 39 Nargund, G. *et al.* Cumulative conception and live birth rates in natural (unstimulated)
677 IVF cycles. *Hum Reprod* **16**, 259-262, doi:10.1093/humrep/16.2.259 (2001).
678 40 Technology, S. f. A. R. (2019).
679 41 Rienzi, L., Vajta, G. & Ubaldi, F. Predictive value of oocyte morphology in human IVF:
680 a systematic review of the literature. *Hum Reprod Update* **17**, 34-45,
681 doi:10.1093/humupd/dmq029 (2011).
682 42 Hassold, T. & Hunt, P. To err (meiotically) is human: the genesis of human aneuploidy.
683 *Nat Rev Genet* **2**, 280-291, doi:10.1038/35066065 (2001).
684 43 Stein, P. & Schindler, K. Mouse oocyte microinjection, maturation and ploidy
685 assessment. *J Vis Exp*, doi:10.3791/2851 (2011).
686 44 Chatot, C. L., Ziomek, C. A., Bavister, B. D., Lewis, J. L. & Torres, I. An improved
687 culture medium supports development of random-bred 1-cell mouse embryos in vitro. *J*
688 *Reprod Fertil* **86**, 679-688, doi:10.1530/jrf.0.0860679 (1989).
689 45 Rieder, C. L. The structure of the cold-stable kinetochore fiber in metaphase PtK1 cells.
690 *Chromosoma* **84**, 145-158, doi:10.1007/BF00293368 (1981).

691

692

693

Fig. 1

A

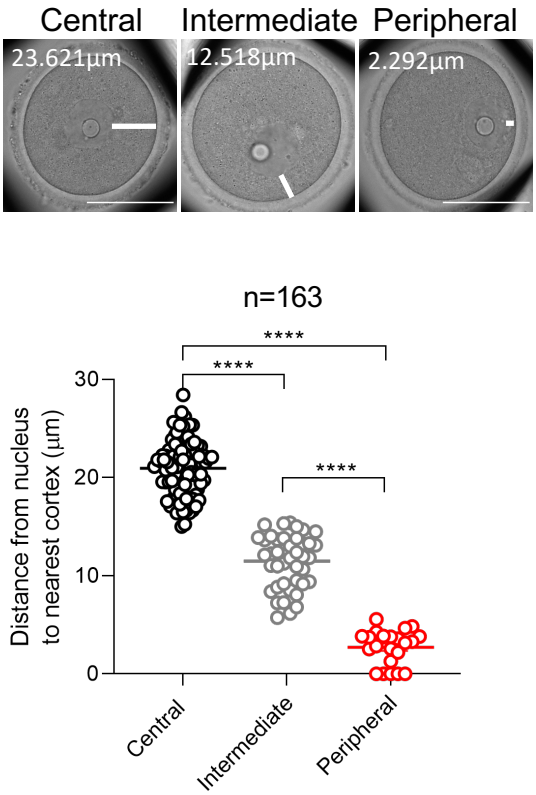
Central
Intermediate
Peripheral
23.621µm
12.518µm
2.292µm
n=163
****
****
****
Distance from nucleus to nearest cortex (µm)
30
20
10
0
Central
Intermediate
Peripheral

B

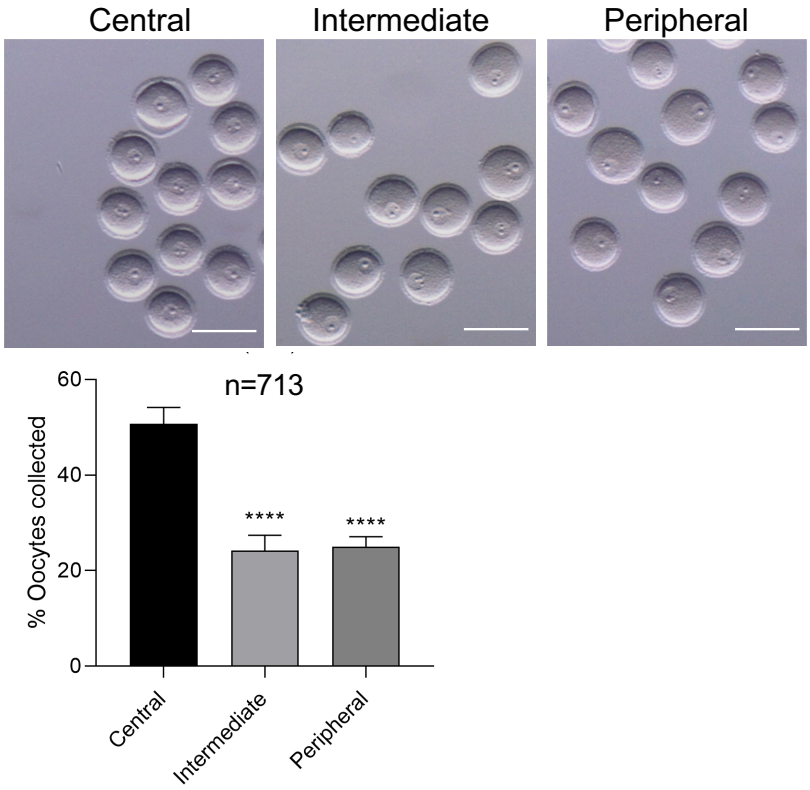
Central
Intermediate
Peripheral
n=713
% Oocytes collected
60
40
20
0
****
****
Central
Intermediate
Peripheral

C

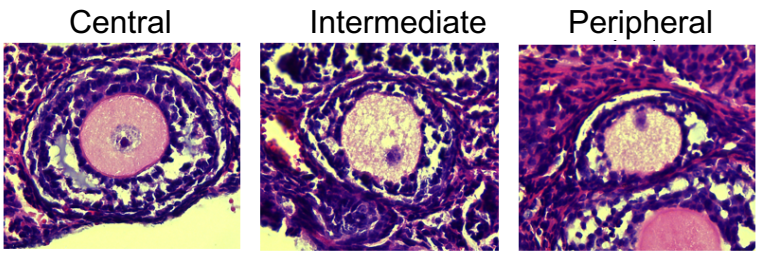
Central
Intermediate
Peripheral

D

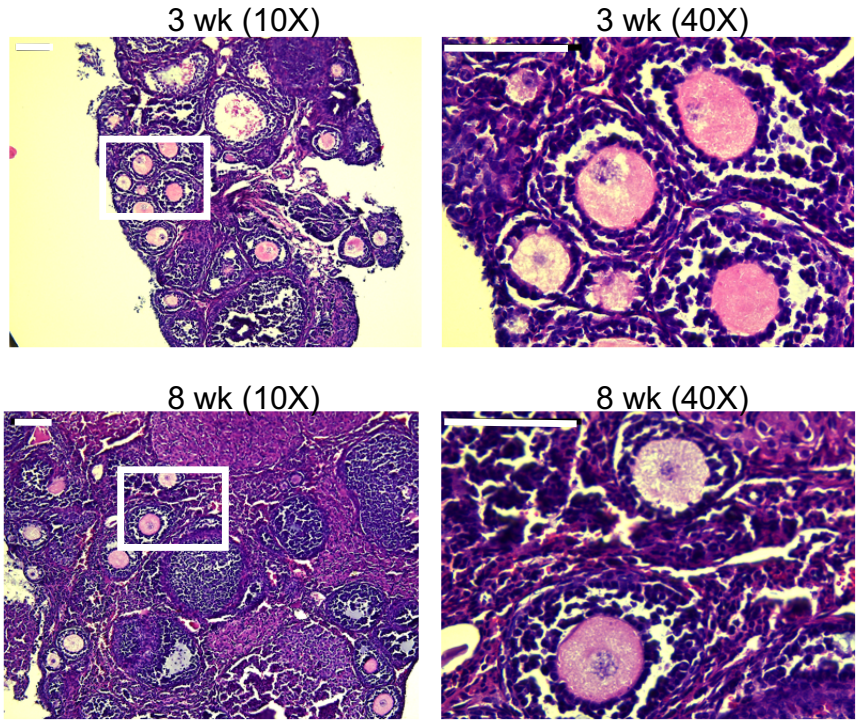
3 wk (10X)
3 wk (40X)
8 wk (10X)
8 wk (40X)

E

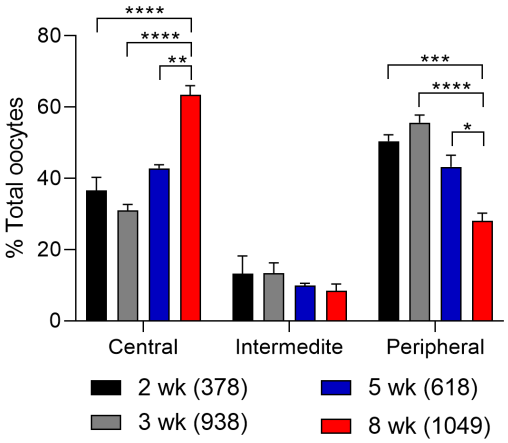
% Total oocytes
80
60
40
20
0
****
****
**
***
****
*
Central
Intermedite
Peripheral
2 wk (378)
3 wk (938)
5 wk (618)
8 wk (1049)

Fig. 2

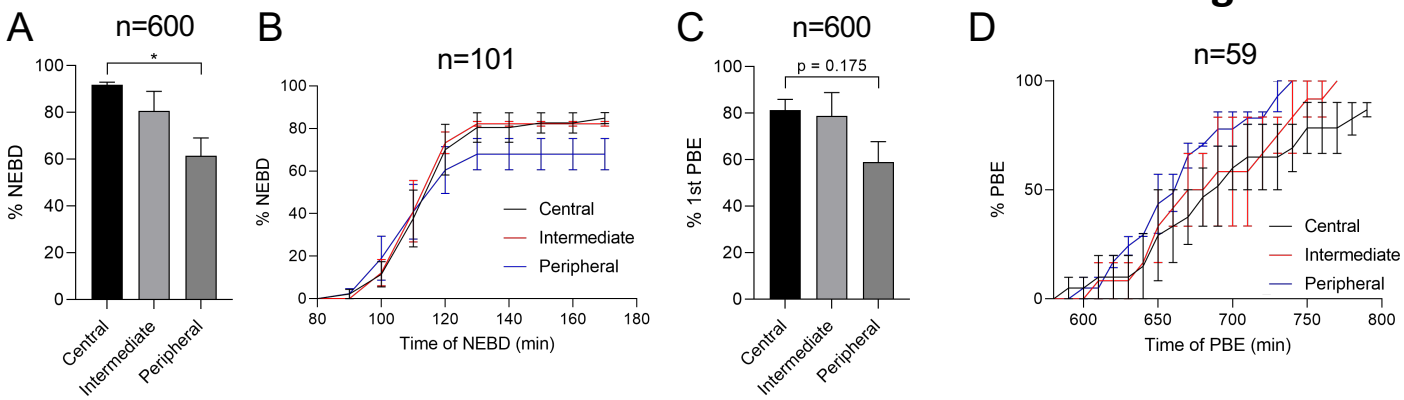
A
n=600
% NEBD
Central
Intermediate
Peripheral
B
n=101
% NEBD
Time of NEBD (min)
Central
Intermediate
Peripheral
C
n=600
p = 0.175
% 1st PBE
Central
Intermediate
Peripheral
D
n=59
% PBE
Time of PBE (min)
Central
Intermediate
Peripheral

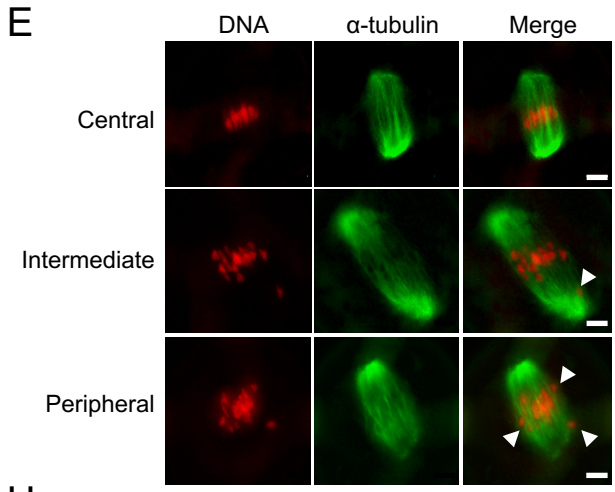
E
DNA
α-tubulin
Merge
Central
Intermediate
Peripheral

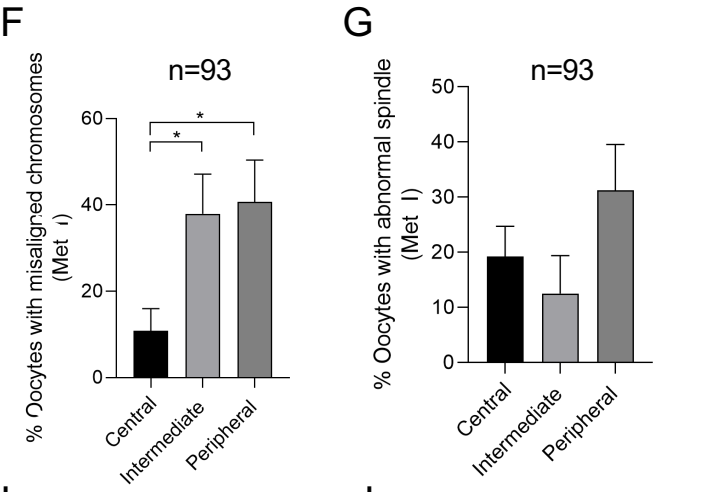
F
n=93
% Oocytes with misaligned chromosomes (Met I)
Central
Intermediate
Peripheral
G
n=93
% Oocytes with abnormal spindle (Met I)
Central
Intermediate
Peripheral

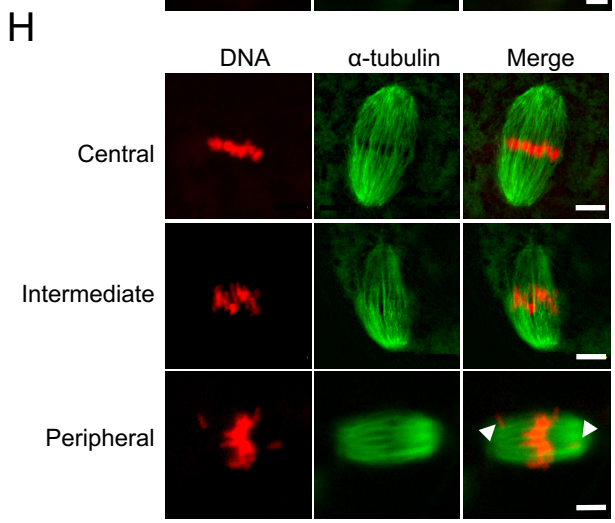
H
DNA
α-tubulin
Merge
Central
Intermediate
Peripheral

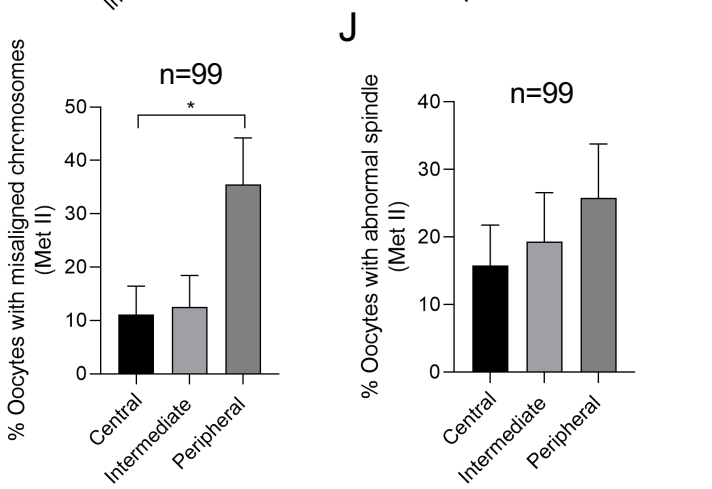
I
n=99
% Oocytes with misaligned chromosomes (Met II)
Central
Intermediate
Peripheral
J
n=99
% Oocytes with abnormal spindle (Met II)
Central
Intermediate
Peripheral

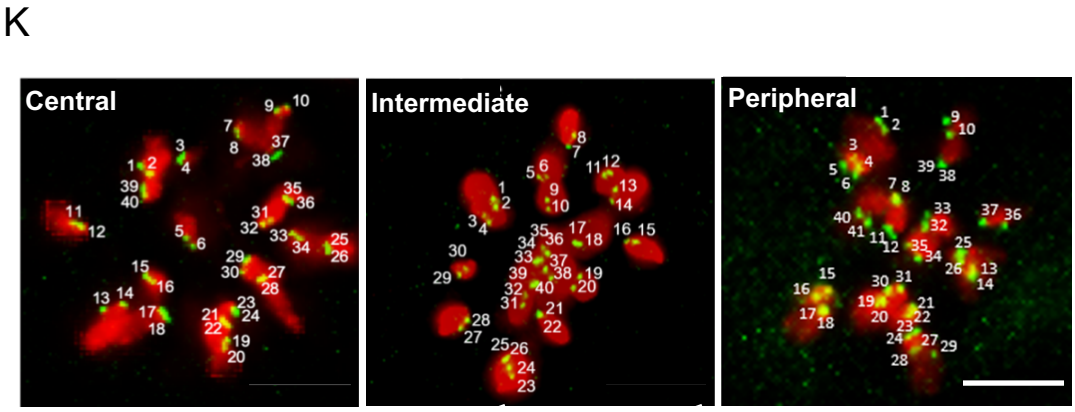
K
Central
Intermediate
Peripheral

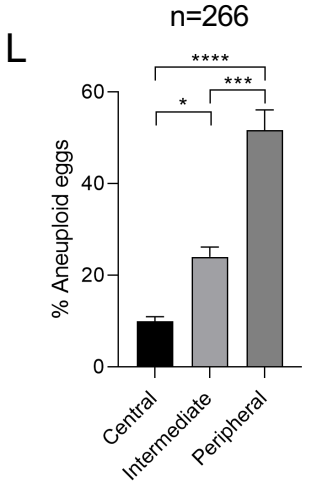
L
n=266
% Aneuploid eggs
Central
Intermediate
Peripheral

Fig. 3

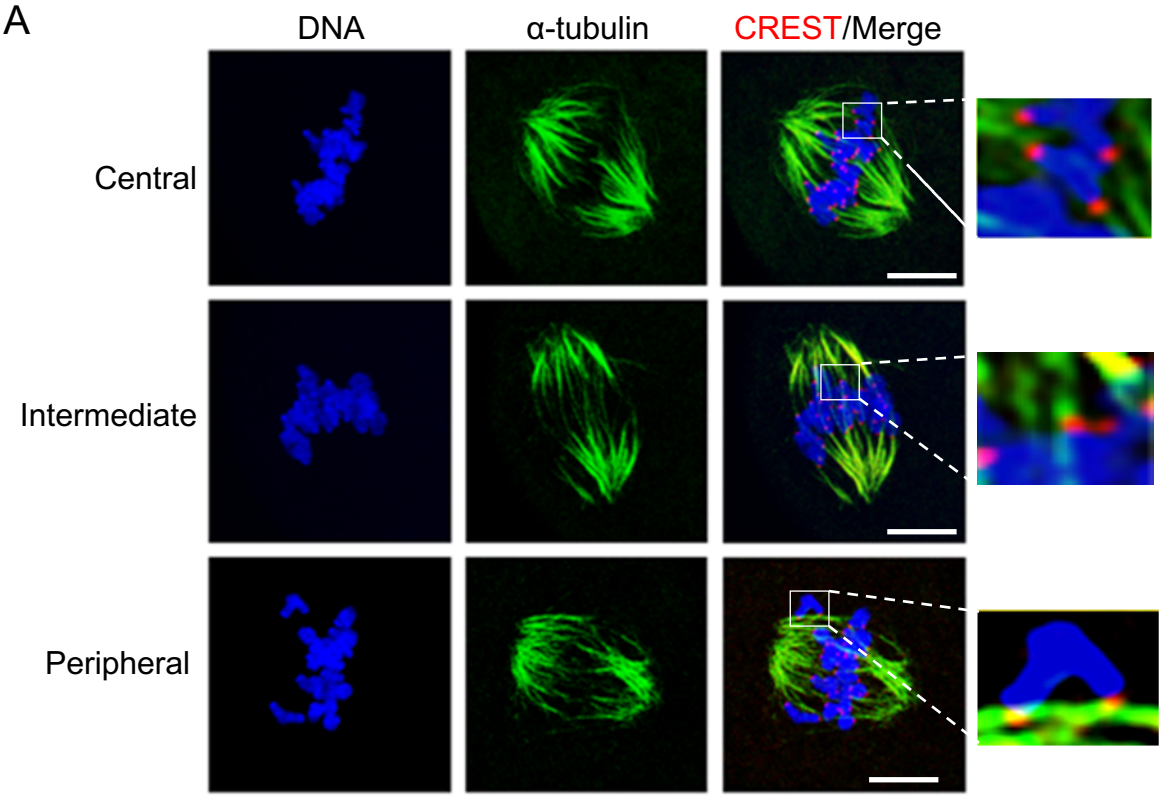
A
DNA
α-tubulin
CREST/Merge
Central
Intermediate
Peripheral

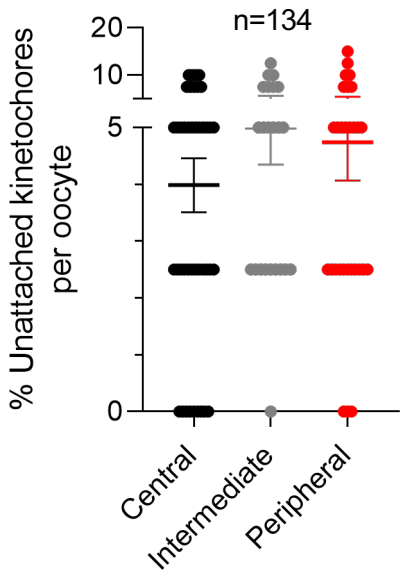
B
n=134
% Unattached kinetochores per oocyte
20
10
5
0
Central
Intermediate
Peripheral

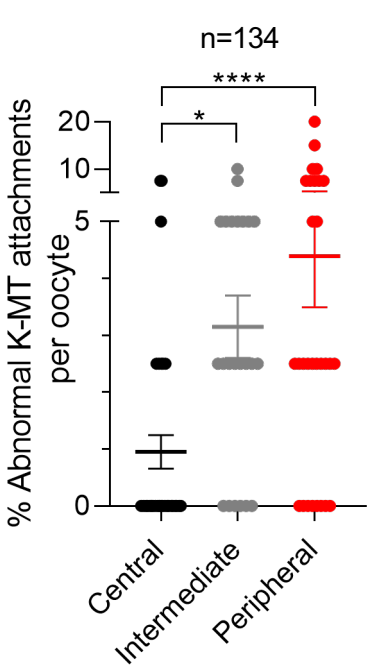
C
n=134
****
*
% Abnormal K-MT attachments per oocyte
20
10
5
0
Central
Intermediate
Peripheral

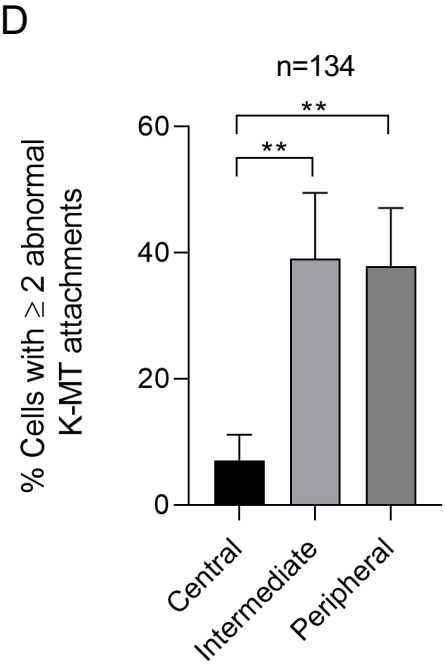
D
n=134
**
**
% Cells with ≥ 2 abnormal K-MT attachments
60
40
20
0
Central
Intermediate
Peripheral

Fig. 4

A

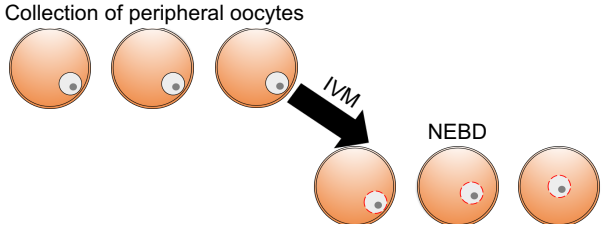

B

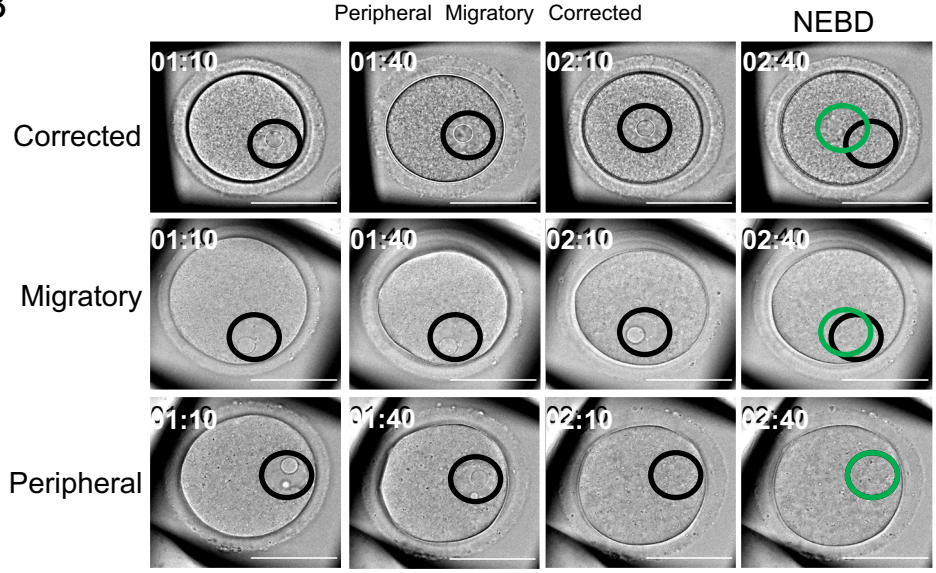

C

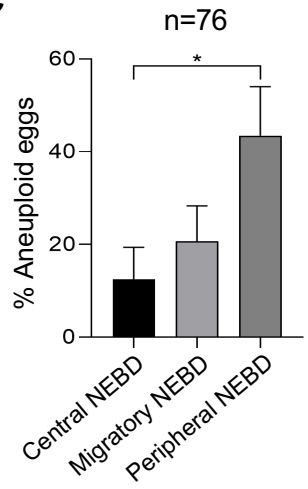

D

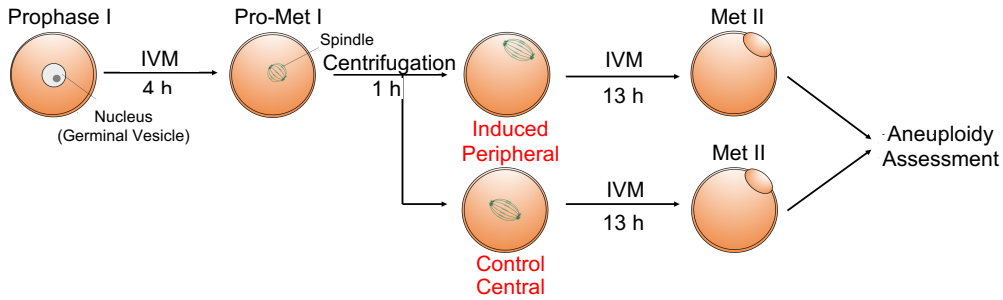

E

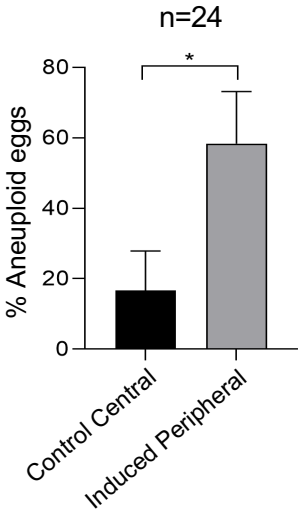

F

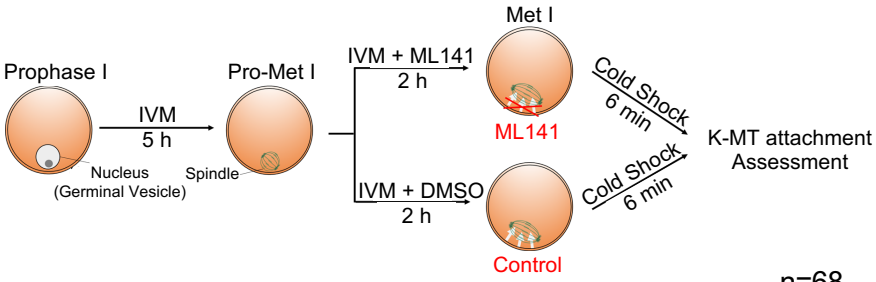

G

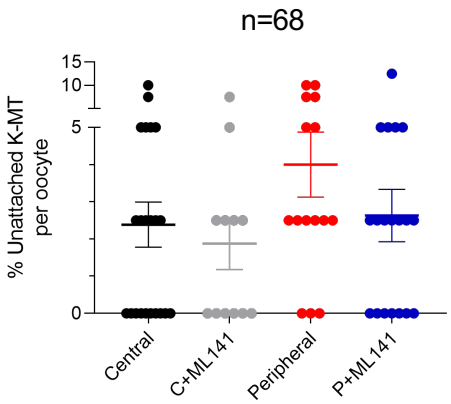

H

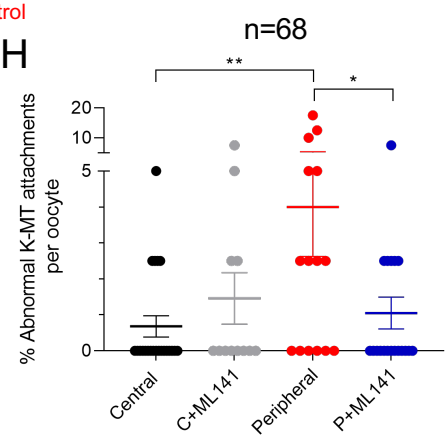

Fig. 5

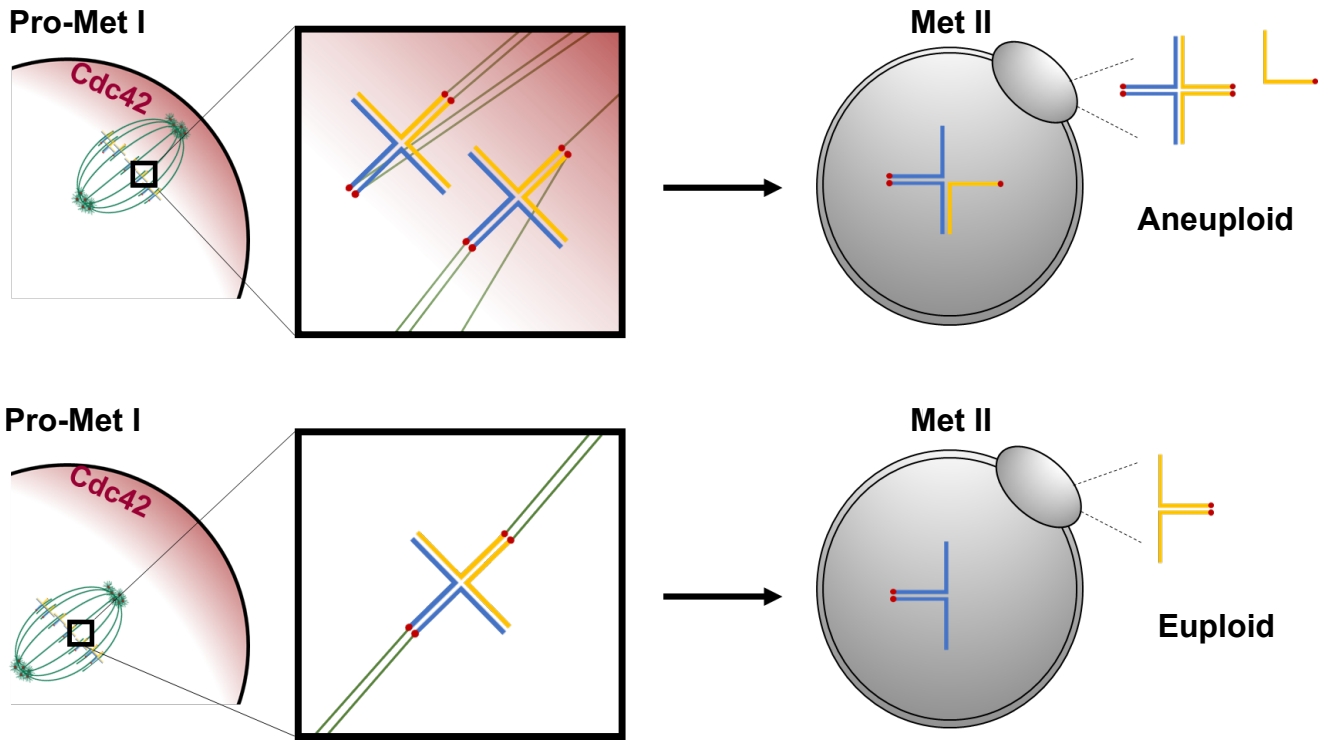
Pro-Met I
Cdc42
Met II
Aneuploid
Pro-Met I
Cdc42
Met II
Euploid

A

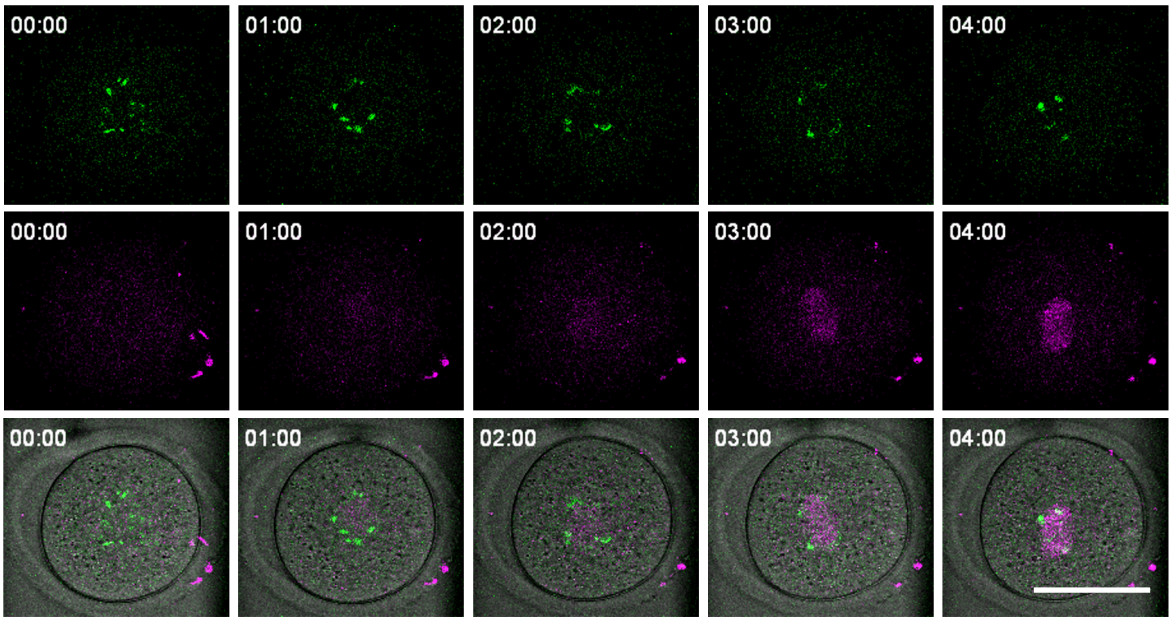

Cep192/SiR-tubulin/Bright-field

B

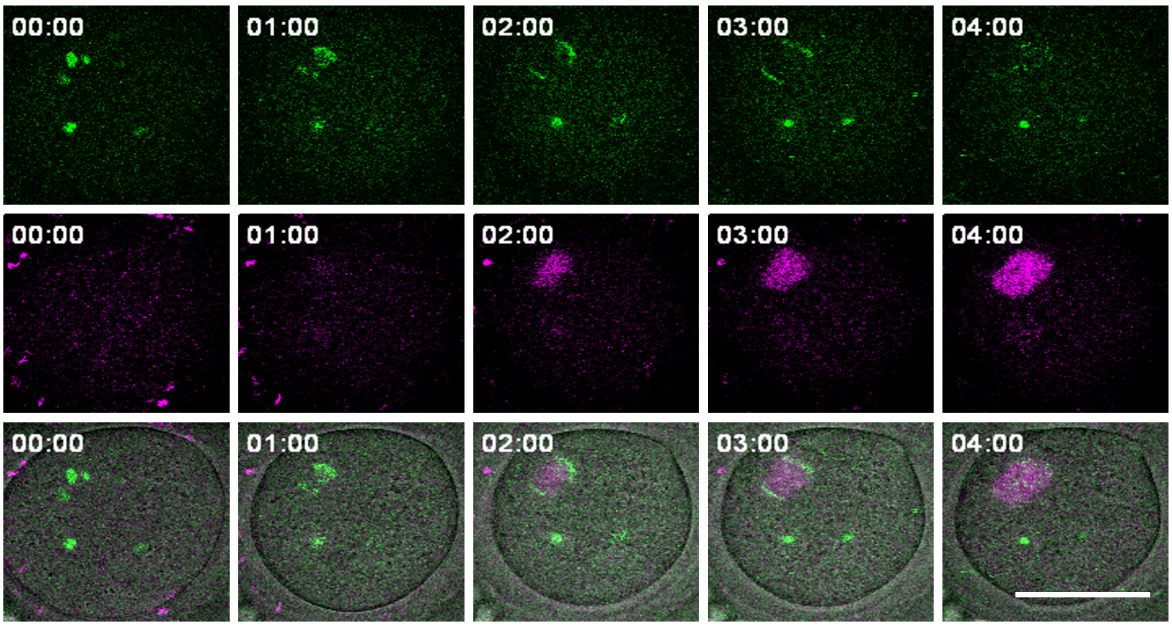

Cep192/SiR-tubulin/Bright-field

Supplementary Figure 1

A

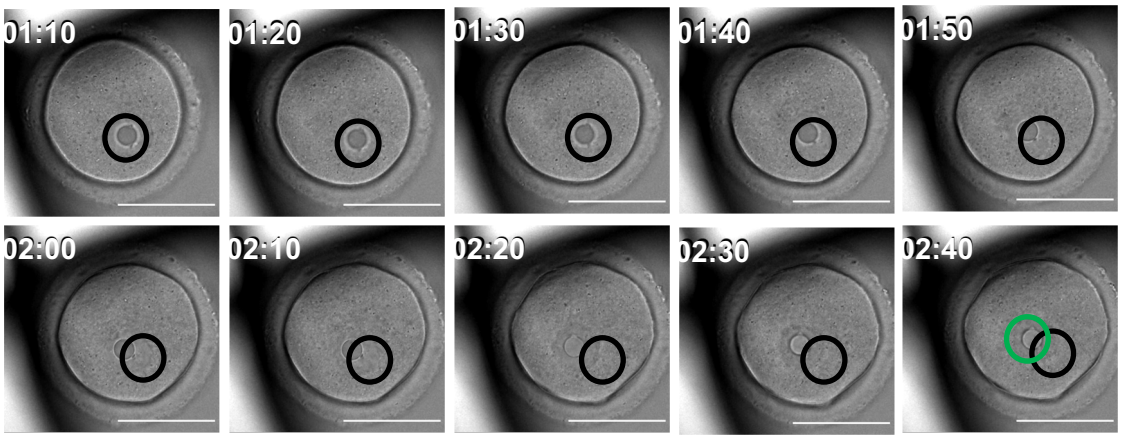

B

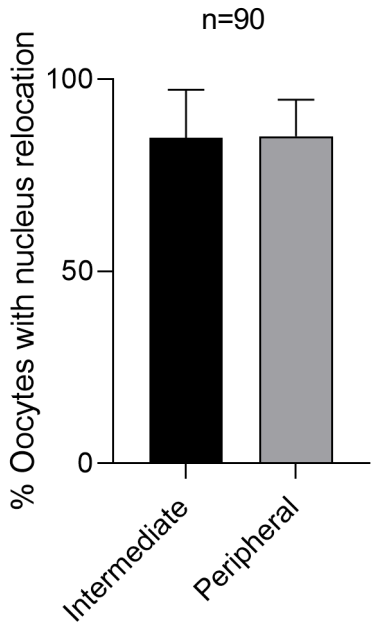

Supplementary Figure 2

A

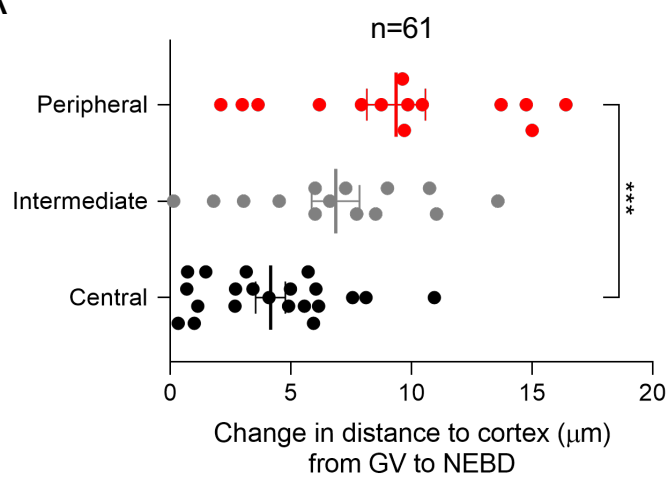

B

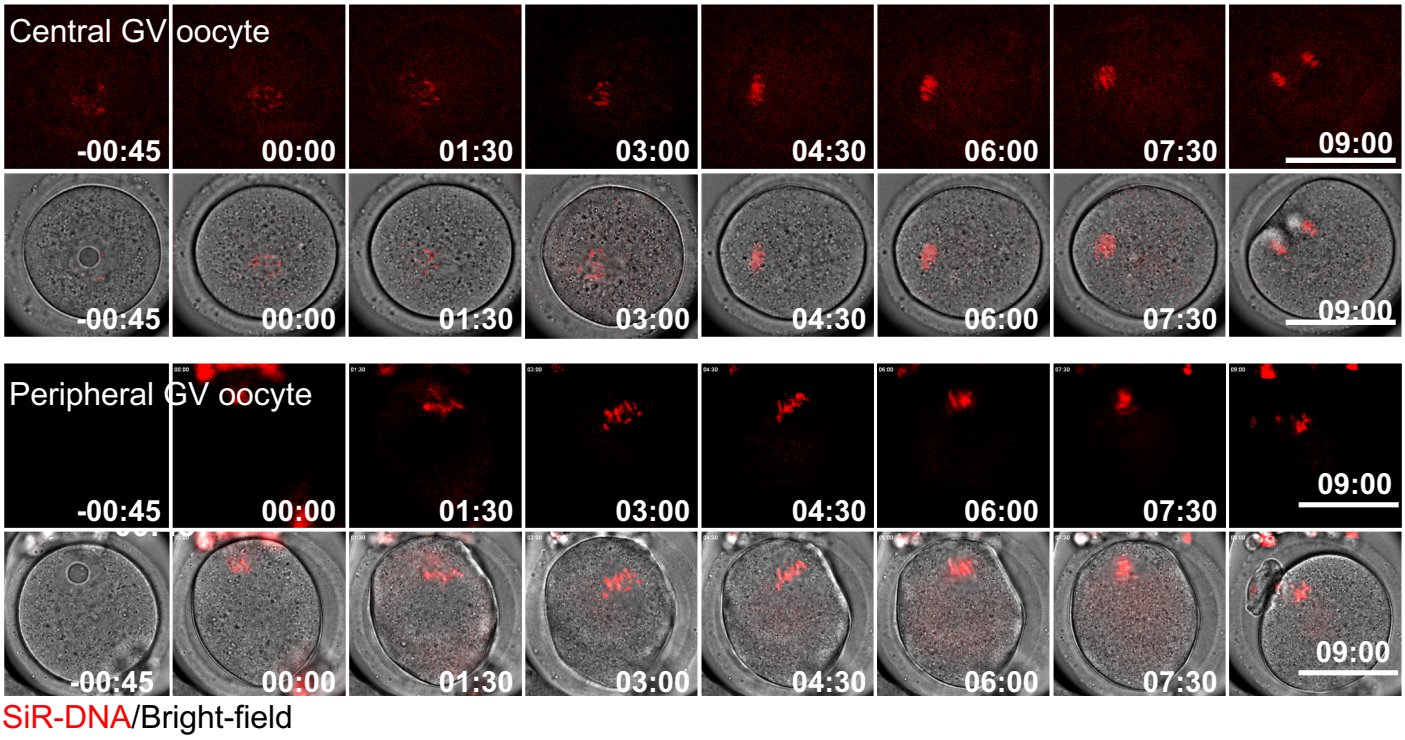

C

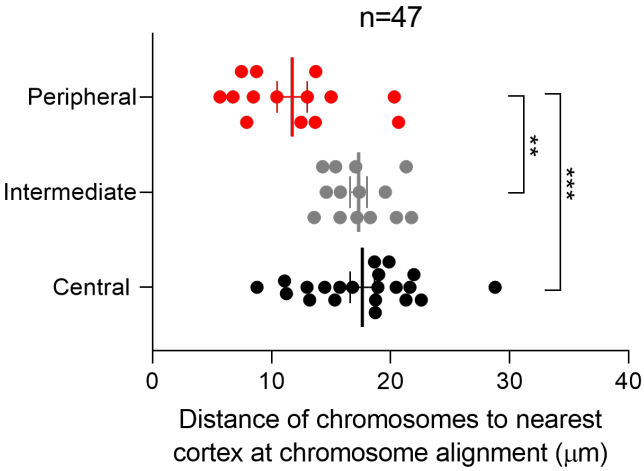

D

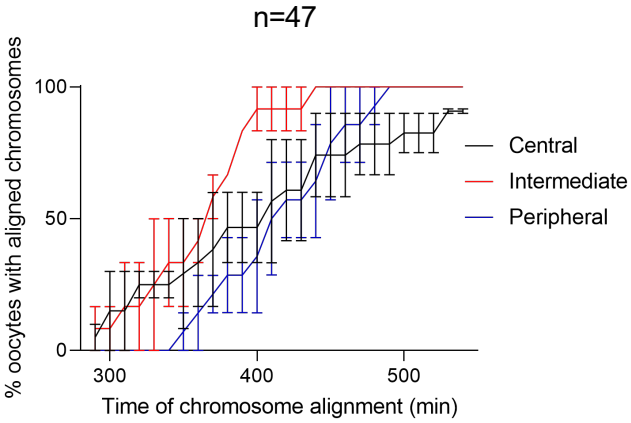

Supplementary Figure 3

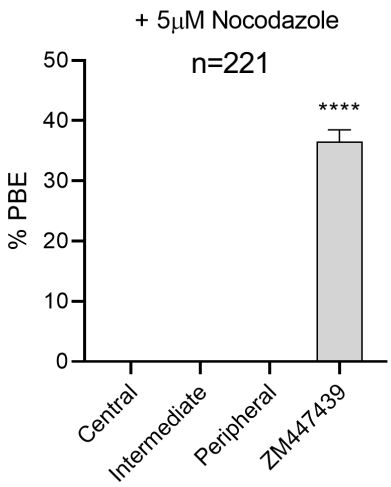

Supplementary Figure 4